Computational pipeline for the generation and validation of patient-specific mechanical models of brain development

Mireia Alenyá, Xiaoyu Wang, Julien Lefèvre, Guillaume Auzias, Benjamin Fouquet, Elisenda Eixarch, François Rousseau, Oscar Camara

Journal Pre-proof

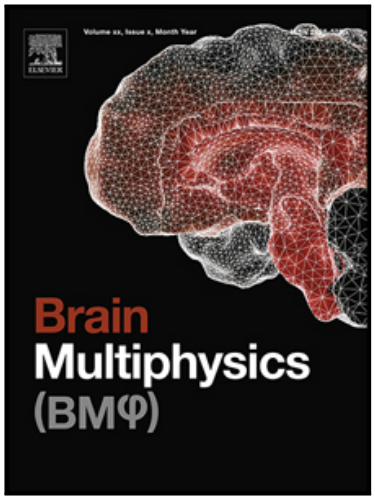

Computational pipeline for the generation and validation of patient-specific mechanical models of brain development

Mireia Alenyá, Xiaoyu Wang, Julien Lefévre, Guillaume Auzias, Benjamin Fouquet, Elisenda Eixarch, François Rousseau, Oscar Camara

PII: S2666-5220(22)00002-8
DOI: https://doi.org/10.1016/j.brain.2022.100045
Reference: BRAIN 100045

To appear in: *Brain Multiphysics*

Received date: 9 October 2021
Revised date: 1 March 2022
Accepted date: 1 March 2022

Please cite this article as: Mireia Alenyá, Xiaoyu Wang, Julien Lefévre, Guillaume Auzias, Benjamin Fouquet, Elisenda Eixarch, François Rousseau, Oscar Camara, Computational pipeline for the generation and validation of patient-specific mechanical models of brain development, *Brain Multiphysics* (2022), doi: https://doi.org/10.1016/j.brain.2022.100045

Computational pipeline for the generation and validation of patient-specific mechanical models of brain development

Mireia AlenyÃă[a,*,1], Xiaoyu Wang[b], Julien LefÃÍvre[c], Guillaume Auzias[c], Benjamin Fouquet[b], Elisenda Eixarch[d], FranÃğois Rousseau[b] and Oscar Camara[a]

[a]*BCN-MedTech, DTIC, Universitat Pompeu Fabra, Barcelona, Spain*
[b]*IMT Atlantique, LaTIM U1101 INSERM, UBL, Brest, France*
[c]*Aix Marseille Univ, CNRS, INT, Inst Neurosci Timone, Marseille, France*
[d]*BCNatal, IDIBAPS, Universitat de Barcelona, Barcelona, Spain*

ARTICLE INFO

Keywords:
brain development
patient-specific modelling
ventriculomegaly
biomechanics
open science
validation
fetal magnetic resonance imaging

ABSTRACT

The human brain develops from a smooth cortical surface in early stages of fetal life to a convoluted one postnatally, creating an organized ensemble of folds. Abnormal folding patterns are linked to neurodevelopmental disorders. However, the complex multi-scale interactions involved in cortical folding are not fully known yet. Computational models of brain development have contributed to better understand the process of cortical folding, but still leave several questions unanswered. A major limitation of the existing models is that they have basically been applied to synthetic examples or simplified brain anatomies. However, the integration of patient-specific longitudinal imaging data is key for improving the realism of simulations. In this work we present a complete computational pipeline to build and validate patient-specific mechanical models of brain development. Starting from the processing of fetal brain magnetic resonance images (MRI), personalised finite-element 3D meshes were generated, in which biomechanical models were run to simulate brain development. Several metrics were then employed to compare simulation results with neonatal images from the same subjects, on a common reference space. We applied the computational pipeline to a cohort of 29 subjects where fetal and neonatal MRI were available, including controls and ventriculomegaly cases. The neonatal brain simulations had several sulcal patterns similar to the ones observed in neonatal MRI data. However, the pipeline also revealed some limitations of the evaluated mechanical model and the importance of including patient-specific cortical thickness as well as regional and anisotropic growth to obtain more realistic and personalised brain development models.

Statement of Significance:
Computational modelling has emerged as a powerful tool to study the complex process of brain development during gestation. However, most of the studies performed so far have been carried out in synthetic or two-dimensional geometries due to the difficulties involved in processing real fetal data. Moreover, as there is no correspondence between meshes, comparing them or assessing whether they are realistic or not is not a trivial task. In this work we present a complete computational pipeline to build and validate patient-specific mechanical models of brain development, mainly based on open-source tools.

1. Introduction

During brain development there is a process of folding of the cerebral cortical surface creating outward (or convex hills) folds known as gyri and inward (or concave valleys) folds called sulci. The resulting cerebral cortex is highly convoluted in humans and large mammals, attaining a large surface area relative to brain volume, as analysed in [26] for 34

*Corresponding author
mireia.alenya@upf.edu (M. AlenyÃă)
ORCID(s): 0000-0002-9548-0873 (M. AlenyÃă)

primate species. Brain/cortical folding mostly occurs during gestational ages (GA) 16-40 [57], following a hierarchical organisation. Primary folds are the largest, deepest and early formed, being progressively subdivided into secondary and tertiary folds [31]. Compared to the huge variations across adult brains, the location and timing of formation of the first folds is remarkably stable [15]. Cortical fold wavelength is also similar between different primate species [26], as it is directly related to cortical bending stiffness (thus on cortical thickness), which does not substantially change across mammalian species [43].

The size and folding of the cerebral cortex have a fundamental impact on brain function [17], with abnormal patterns (e.g., reduced or excessive folding that is defined as lyssencephaly and polymicrogyria, respectively) leading to severe intellectual disability [25]. Due to its clinical relevance, it is then essential to better understand the relation between cortical malformations and neurodevelopmental disorders. Recent studies (e.g., [21, 58]) have exposed that mechanical forces play an important role in the generation of characteristic folding patterns. More precisely, several works [12, 68, 59] showed that differential tangential growth between different layers of the cortex (i.e., grey and white matter) generates a compressive stress that is sufficient to induce buckling. Additionally, several studies have demonstrated that axonal tension within fibres in the white matter plays a key role in modulating folds' shape [60, 70, 5]. However, the interactions between the many multi-scale developmental processes involved in the dynamics of cortical folding remain to be clarified [66].

Several computational models of brain development have been proposed in the literature [60, 44, 4, 44, 21, 18, 72], contributing to improve our knowledge about the mechanisms underlying cortical folding. They are mainly based on different continuum mechanics theories. The interested reader is refereed to [24, 10] for a comprehensive review of brain (tissue) mechanics and its modelling. For instance, the theory of finite elasticity was used in [24] to prove that growth induces elastic instability with buckling modes of different wavelengths depending on the growth parameters and thickness of the shell, which naturally relates to the process of brain folding. The two most explored theories on cortical folding are based on axonal tension and differential growth hypothesis. The former one, first proposed in [61], is based on the assumption that axons connecting neurons in white matter mechanically pull highly interconnected regions of grey matter together to form gyri. The same author recently proposed a revision of the theory that includes tangential tension and sulcal zipping forces in the outer cortical margin and tension in the white matter core, together competing against radially-biased tension in the cortical grey matter [62]. On the other hand, the differential growth theory, proposed in [50], is based on a larger growth rate of cortical tissues compared to white matter, thus leading to mechanical buckling shaping the cortex. Tallinen et al. [58, 59] extended experimental studies of differential growth to 3D, using hemispheres of layered swelling gel. These authors also performed numerical simulations of growing hyperelastic materials starting from an idealised smooth fetal brain 3D mesh, obtaining results reasonably matching

experimental observations.

Models only based on uniform surface growth on an elastic foundation have difficulties to reproduce the location and orientation of primary folds, nor the growth of white matter. Toro et al. [60] added stress-induced growth in a folding model by including radial and discrete viscoelastic fibres connected to an expanding elastic ring, which represented the cortical plate. Bayly et al. [5] derived an analytical formulation of the effects of relative growth rate on the folding wavelength, by representing the sub-cortical region as a continuous viscoelastic core. Budday et al. [11], modelled the human brain as a morphogenetically growing outer surface and a stretch-driven growing inner core, combining both axonal tension and differential growth hypotheses. The authors confirmed that the ratio between inner and outer layers' growth rates influenced folding wavelength. This model was extended by Holland et al. [27] to study cortical anisotropic growth, due to the preference of axons to elongate in their axial direction. As an alternative, Wang et al. [64] recently proposed to link cortical growth rate to mean curvature variations, achieving distinct gyral or sulcal growth. Finally, Zarzor et al. [72] are pioneering the development of multi-scale models of brain development, coupling cellular processes with cortical folding, where cell properties (e.g., migration velocity, diffusivity) influence cortical growth.

A major limitation common to all the proposed models is that they have only been applied to synthetic simplified geometries (e.g., disks, ellipsoids, spheres) [60, 11, 67] or to simplified brain anatomies [58, 27, 59, 66]. Experiments with synthetic data are required as part of the model validation stage to characterize the sources of errors and have better control over their parameters. However, the integration of patient-specific longitudinal data of brain development is key for assessing the accuracy of resulting predictions, through model validation and parameter optimisation with data assimilation processes. Appropriate accuracy metrics are consequently required to compare simulation results and observations. Obtaining imaging data to explore human brain development at different time-points in fetal life is nonetheless challenging, unlike for other species such as ferrets, where cortical folding and white matter maturation take place during the first month of life [3]. Ultrasound [69] and magnetic resonance images (MRI) [6] of the fetal brain are increasingly providing insights on brain development in vivo, but still with insufficient spatial resolution (from ultrasound images) or requiring advanced image processing pipelines (in MRI) to compensate acquisition reconstruction problems due to motion.

Another factor hampering the progress in patient-specific brain development models is the lack of openly shared pipelines including all the required steps. The neuroimaging community is steadily promoting Open Science and reproducible research, with numerous established tools for brain MRI data harmonization and processing (e.g., Clinica [53]), some of them for the description of cortical folding in healthy and pathological human brains, as well as in other species (e.g., PRIME-RE [41]). Unfortunately brain mechanical models are not integrated into the existing pipelines

yet, despite the availability of solvers used in some successful studies [59, 67][1][2].

In this work we present a complete computational pipeline to build and validate patient-specific mechanical models of brain development, mainly based on Open Source tools. Starting from the processing of fetal brain MRI, personalized finite-element methods 3D meshes are generated, where biomechanical models are run to simulate brain development. Several metrics are then used to compare simulation results with neonatal data from the same subjects, on a common reference space built to integrate data from different individuals and time-points. The pipeline has been applied to a cohort of 29 subjects where fetal and neonatal MRI were available, including controls (n = 16) and ventriculomegaly (n = 13) cases.

2. Materials and methods

A scheme of the proposed pipeline is illustrated in Figure 1 and described in sections 2.2-2.4. The first step of the pipeline is the brain tissue segmentation of fetal and neonatal MRI of the same subject. The grey matter (or cortical surface) label is then the basis for building finite element method (FEM) meshes, which are later refined if required to ensure model convergence. Cortical thickness maps and brain parcellation are also derived from MRI data. The fetal meshes and patient-specific cortical thickness maps are subsequently set as input for the computational model that simulates brain growth and folding until the GA at which neonatal real data was available for that subject. Finally, neonatal simulations and observations are compared through global and local metrics.

2.1. Clinical imaging database

The clinical imaging database was composed of longitudinal brain MRI data from a cohort within a research project on isolated non-severe ventriculomegaly (INSVM), carried out at Hospital ClÃŋnic in Barcelona, Spain. Approval was obtained for the study protocol from the Ethics Committee of the Hospital ClÃŋnic in Barcelona, Spain (HCB/2014/0484) and all patients gave written informed consent.

Fetal ventriculomegaly (VM) occurs in around 1 out of 10 pregnancies [55]. It is defined as a dilation (≥10 mm) of one or both lateral ventricles, measured in 2D in ultrasound images, being 6-8 mm the normal width in fetuses [7]. In the absence of other anomalies, it is called isolated ventriculomegaly. Studies [56, 33, 7] have confirmed alterations in folding in fetuses with ventricular enlargement, therefore underlining the clinical relevance of understanding the gyrification process.

We finally included 31 subjects from a larger cohort of 81 subjects (38 controls and 43 with INSVM), the ones where both fetal and neonatal reconstructed MRI were available. Two subjects were excluded due to inaccurate segmentation results (see Section 3.1). The demographic information of the 29 subjects included in our study is summarised in Table

[1] http://users.jyu.fi/~tutatall/codes.html
[2] https://github.com/rousseau/BrainGrowth

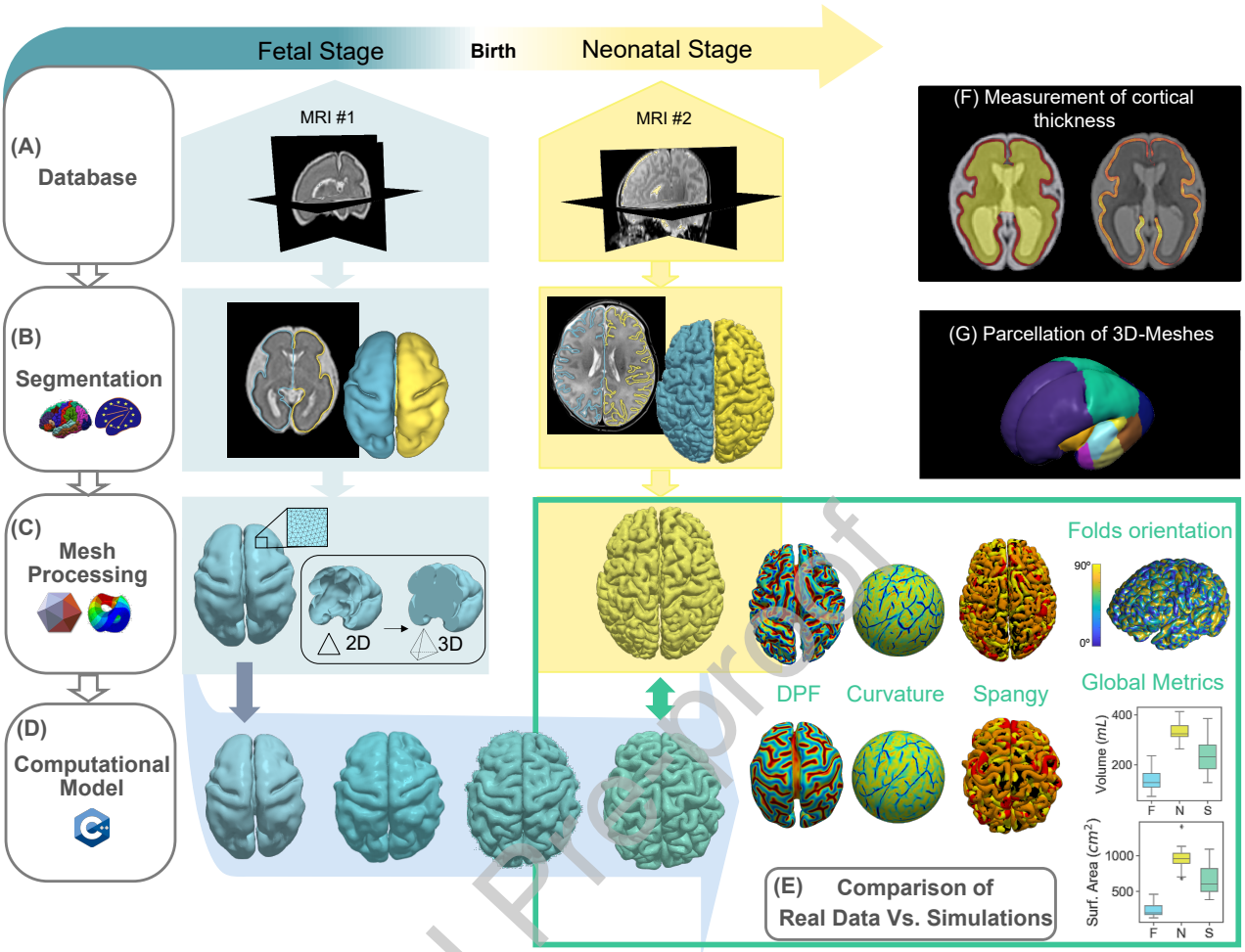

Figure 1: Scheme of the computational pipeline for patient-specific brain mechanical model generation and validation. (A) Example of fetal and neonatal magnetic resonance imaging (MRI) scans of one subject. Background of fetal and neonatal MRI processing is coloured in blue and yellow, respectively. (B) Image segmentation was performed with the Developing Human Connectome Project (dHCP) structural pipeline [40]. (C) Mesh processing was performed with Meshmixer, using Netgen to generate the 3D fetal meshes. (D) With the fetal geometry (gestational age, GA, of 28) as starting point, the computational model simulated brain development. Predicted meshes of GA 32, 36 and 40 are displayed. (E) Comparison between the neonatal real and simulated meshes using global and local metrics. DPF: Depth potential function. (F) Measurement of cortical thickness from images. (G) Parcellation of 3D meshes.

1. In addition, ground-truth segmentations performed by clinicians were provided for 13 out of those 31 fetal images.

T2-weighted MR imaging was performed on a 1.5-T scanner (Siemens Magnetom Aera syngo MR D13; Munich, Germany) with a 8-channel body coil, resulting in images with a 2.5 mm of slice thickness, a 280ÃŮ280 mm field of view and a voxel size of 0.5ÃŮ0.5ÃŮ2.5 mm^3. Multiple orthogonal acquisitions were performed for each subject: 4 axial, 2 coronal and 2 sagittal stacks. From these 8 stacks of thick 2D slices, final 3D motion-corrected reconstructions were obtained; subsequently, brain location and extraction were performed with the methods presented in [28]. A high-resolution 3D volume reconstruction was then conducted using the approach proposed in [32].

Table 1
Clinical characteristics of the cohort.

Gestational / Postmenstrual Age ($mean \pm SD$)	
at Birth (week)	39.73 ± 1.12
at MRI 1 (week)	29.25 ± 2.74
at MRI 2 (week)	43.51 ± 1.71
Gender n (%)	
Male	22 (75.86%)
Female	7 (24.14%)
Controls / Ventriculomegaly Cases n (%)	
Controls	16 (55.17%)
Ventriculomegaly	13 (44.83%)
Fetal MRI Onset n (%)	
Early (< 30)	20 (68.97%)
Late (> 30)	9 (31.03%)
Ethnicity n (%)	
African	2 (6.90%)
Asian	1 (3.45%)
Caucasian	23 (79.31%)
Latin American	3 (10.34%)

2.2. Medical image processing

Cortical surface geometries were obtained from neonatal images using the Developing Human Connectome Project (dHCP) structural pipeline [40]. For the fetal cases, a modified version of the dHCP pipeline was used, integrating a fetal-specific atlas [23] to permit segmentation of images taken in early gestation.

We used the ground-truth labels from 13 subjects to evaluate the accuracy of the automatic segmentation method, as illustrated on Figure 2. The obtained results were compared both visually, by displaying them using Paraview[3] and 3DSlicer[4], and quantitatively, by computing the Dice Coefficient, Hausdorff Distance (HD) and Volume Similarity (VS) measures, as follows:

$$Dice = \frac{2|GT \cap X|}{|GT| + |X|}, \tag{1}$$

where GT represented the ground-truth and X the obtained segmentation, so $GT \cap X$ corresponded to their intersection; $HD = max(h(GT, X), h(X, GT))$, where $h(GT, X)$ was the directed Hausdorff distance, given by $h(GT, X) = \max_{GT \in X} \min_{x \in X} \|gt - x\|$, being $\|gt - x\|$ the Euclidean distance between points gt and x;

$$VS = 1 - \frac{||GT| - |X||}{|GT| + |X|}. \tag{2}$$

[3] https://www.paraview.org/
[4] https://www.slicer.org/

As described in [39], the output of the dHCP structural pipeline included 2D meshes and associated feature maps for left and right hemispheres. The different meshes corresponded to the external grey matter, the interface between grey and white matter and the mid-thickness surface. In addition, an inflated, very inflated and spherical versions of the surfaces were provided. These surfaces had the exact number of vertices and faces as the original mesh and were used for visualisation and comparison purposes. The feature maps obtained for all subjects were: sulcal depth, cortical thickness, mean curvature and brain parcellations.

Cortical thickness (H) was estimated on fetal MRI using the Pyezzi python library[5], computing the thickness of tissues between the internal and external borders of the grey matter segmentation (Figure 1.F) [71].

2.3. Mesh processing

The FreeSurfer[6] and Meshmixer[7] softwares were used for the format conversion and manipulation of 2D surface meshes resulted from the brain segmentation. Especially to combine both brain hemispheres into one single geometry, repair surface imperfections (i.e., topology correction of defects such as handles or holes, artifacts, and fix non-manifold edges and self-intersecting faces) and to define an appropriate density of mesh elements (Figure 1.B). The number of mesh elements was empirically defined with a minimum of 1 M tetrahedra, since folding configuration (i.e., size and number) did not substantially change with more elements, following prior mesh convergence studies in [67]. Netgen[8] was used to generate volumetric tetrahedral meshes through the Delaunay triangulation Method (Figure 1C). The mean value and standard deviation of the mesh density was of 1.89 ± 0.25M tetrahedra.

Defining point-to-point correspondence across meshes is challenging. The anatomical multimodal surface matching (aMSM) technique [52, 51] was originally proposed as a spherical registration tool to define spatial correspondences between two anatomical surfaces, each projected onto a sphere. The alignment can be driven by any feature map extracted from the two surfaces to match. In our pipeline, we used the mean curvature and the Depth Potential Function (described below in Section 2.5.2) as the guiding feature maps. The registration process involved a resampling of the meshes which induced a one-to-one correspondence across the vertices of the matched surfaces, such that each vertex corresponded to the same anatomical location across the surfaces.

The aMSM tool was also used to generate atlases from groups of meshes, as in [21]. Cortical surfaces were resampled to a standard 158,762-vertex mesh and averaged (with Workbench Command tools[9]) to create a preliminary atlas. Original surfaces were then registered to the preliminary atlas using aMSM (with default parameters) and averaged to obtain the final atlas. Atlases were also created for separated hemispheres by resampling meshes to a standard 79212-vertex mesh.

[5] https://gitlab.inria.fr/ncedilni/pyezzi
[6] https://surfer.nmr.mgh.harvard.edu/
[7] https://www.meshmixer.com/
[8] https://ngsolve.org/
[9] https://www.humanconnectome.org/software/workbench-command

2.4. Brain mechanical model

We evaluated the finite-element model proposed by Tallinen et al. [58, 59], further modified by [66], which simulates a realistic brain folding process. The C++ codes were open-source [10]. The model was built on the assumption that folding appears due to the instability produced by the different growth rates in interfacing materials; if one grew faster than the other (grey and white matter, respectively), the system would become unstable and buckle.

2.4.1. Constitutive equations

The cortical tissue was modelled as a compressible neo-Hookean material, with strain energy density function:

$$W = \frac{\mu}{2}[Tr(FF^T)J^{\frac{-2}{3}} - 3] + \frac{\kappa}{2}(J-1)^2, \tag{3}$$

μ and κ being the shear and bulk modulus, respectively, F the deformation gradient and $J = detF$. As defined in [59, 67] we assumed $\kappa = 5\mu$, which corresponded to a modestly compressible material. As the model was based on differential growth theory, the ratio between grey and white matter shear stresses was the important parameter to fix. Based on stiffness micro-indentation measurements performed on ferret brains by Xu et al. [70], we assumed the modulus ratio between cortical layer and white matter region to be $\mu/\mu_{white} = 0.86$. The Cauchy Stress was given by:

$$\sigma = \frac{1}{J}\frac{\partial W}{\partial F}F^T. \tag{4}$$

Surface traction of each tetrahedral deformed face was given by $s_i = -\sigma n_i$, with n_i being face normals. Normal forces were obtained by distributing traction of each face equally for its three vertices.

Contacts at the brain surface were modelled via penalty-based vertex-triangle contact processing [16]. If a superficial face and node were closer than a threshold and the computed elastic force would bring them even closer, a contact force would prevent nodes from penetrating element faces.

In the evaluated model, the deformation gradient equation integrated the relative tangential growth (G), being defined as: $F = A(G\widehat{A})^{-1}$.

2.4.2. Growth kinetics

The relative tangential growth tensor G described the tangential expansion perpendicular to the normal vector $\hat{n}$ of the tetrahedron. It was obtained by $G = gI + (1-g)\hat{n}\otimes\hat{n}$, where g was the relative tangential expansion ratio of the cortical layer with respect to the white matter zone. It stepped smoothly from grey ($g = 1+\alpha_t$) to white matter ($g = 1$)

[10] http://users.jyu.fi/~tutatall/codes.html

as follows:

$$g = 1 + \frac{\alpha_t}{1 + e^{10(\frac{y}{H} - 1)}}, \tag{5}$$

where y was the distance from the top surface, H the cortical thickness and α_t the growth rate. The latter was defined as $\alpha_t = (\sqrt{8} - 1)t$ and t as the time in the model, which ranged from 0 to 1. It was experimentally parameterised, according to gyrification index values measured on real folded brains [1, 65]. The equation that related t of the model with gestational age was:

$$t = 0.987e^{-e^{-0.134(GA - 29.433)}}. \tag{6}$$

Along simulation time-steps, the evaluated model imposed a linear increase of cortical thickness, H, with the following expression: $H = H_i + \beta t$. β was empirically defined in [66] to be equal to 0.3 and H_i was set to the chosen initial global patient-specific cortical thickness. The volumetric mesh was built to include all brain tissue inside the grey matter (GM), including the white matter (WM). Each GM and WM element of the mesh was then identified based on its distance from the top surface and H, which varies throughout the simulation, to determine the different material properties of the different brain tissues.

2.4.3. Kinematics of finite growth

As described in [58], the energy of the system was minimized by damped second-order dynamics using an explicit solver for quasi-static equilibrium of the system:

$$v_{t+dt} = v_t + \frac{f_t - \gamma v_t V_n}{m} dt, \tag{7}$$

where $\gamma v_t V_n$ was the damping force, γ the viscous damping of value $\gamma = 0.05$, v_t the velocity and V_n the nodal volume. f_t was the combination of the elastic and contact forces, dt the time step, $m = 10a^3$ the nodal mass and a the mesh spacing in the initial configuration. Positions of the nodes of the mesh at the next time step were computed by:

$$x_{t+dt} = x_t + v_{t+dt} dt. \tag{8}$$

2.5. Validation

2.5.1. Global metrics

Several global metrics, computed using the python package Surface anaLysis And Modeling (SLAM) [11], were estimated to analyse and compare fetal, neonatal and simulated grey matter meshes. First, the surface area was computed as the sum of the area of all the triangles of the 2D mesh. Second, the volume was computed as the surface integral, corresponding to the whole volume enclosed in the 2D mesh of the grey matter. Third, the 3D gyrification index (3D-GI) was computed as in [67], by dividing the area of the mesh by the area of its smooth "convex hull" generated with SLAM.

2.5.2. Local metrics

Curvature

The curvature of the analysed grey matter meshes was calculated in two different ways. First, we used the python library SLAM to obtain the curvature based on the Rusinkiewicz estimation [54], and further compute the non-dimensional curvature (K^*), as defined in [29] and [21]. The Rusinkiewicz-based method defined the mean curvature of a vertex as the average of the two principal curvatures (directions where the normal curvature reached its minimum and maximum), which were the eigenvalues of the vertex normal curvature tensor computed as:

$$II = (u', v') \begin{pmatrix} K_1 & 0 \\ 0 & K_2 \end{pmatrix} \begin{pmatrix} u' \\ v' \end{pmatrix}, \tag{9}$$

where K_1 and K_2 were the eigenvalues and (u', v') the principal directions [54, 67]. The non-dimensional mean curvature was then computed by multiplying $K^* = KL$, where $L = \sqrt{SA/4\pi}$ being SA the total cortical surface area. Second, the Workbench command tools[12] were used to compute the curvature based on [38]. This second alternative was only applied for surface registration in the aMSM and the computation of the depth potential function (see below) due to its low computational cost.

Depth potential function

The depth potential function (DPF), based on [8] and computed with SLAM, was also used to characterise grey matter meshes. DPF is a measure of the average convexity of the cortical mesh. It was defined as the scalar function that had the closest mean curvature to the original surface in a least-square sense, also being spatially regular. The DPF computation was obtained solving the time-independent Poisson's equation. The curvature metric based on [38] was used as an input for computing the DPF.

[11] https://github.com/brain-slam/slam
[12] https://www.humanconnectome.org/software/workbench-command

Spectral analysis of gyrification (SPANGY)

The SPANGY [22] method performed a spectral decomposition of the mean curvature of the grey matter meshes, based on the Laplace-Beltrami operator eigenfunctions. It allowed the parcellation of the cortical surface in 7 ordered spatial frequency bands (B0-B6) according to fold-related variations in curvature. As described in [22], the bands B1-B3 were related to global brain shape, while bands B4-B6 (folding bands) were associated to primary, secondary and tertiary folds. The sum of all the power accumulated in bands B1-B6 was defined as the Analysed Folding Power (AFP). For comparison purposes the power spectrum in each band was divided by the AFP to compute the relative folding power. The SPANGY code (MATLAB) was provided by the authors.

Orientation of folds

As proposed in [67], we calculated the angle between the gradient of Fiedler vectors [35] and the principal directions of curvatures [47] to characterise and compare the orientation of the folds on simulated and real meshes. The Fiedler vector was defined as the first non-constant eigenfunction of the Laplace-Beltrami operator and allowed to describe the longitudinal extension of surfaces. Extrema of Fiedler vectors were the most distant points within a geometry and its contour lines were cuts on the elongation axis. The direction of elongation was defined as the gradient of the Fiedler vector that was orthogonal to the contour lines. The principal directions of the curvatures were the corresponding eigenvectors of the curvature tensor. The folding orientation angles were obtained by the scalar product between the gradient of the Fiedler vector and the principal directions of the curvatures [67].

To quantify the uniformity of the angular distribution of folds the Kullback-Leibler (KL) divergence or also called relative entropy was used. It was used to measure differences between two probability distributions. The KL divergence from probability distribution P to probability distribution Q was defined as:

$$D_{KL}(P||Q) = \sum_i P(i) log \frac{P(i)}{Q(i)}. \tag{10}$$

In our study, P corresponded to the fold angular distributions on the folded surface while Q represented the theoretically uniform distribution of fold angles [67]. The code to compute the orientation of folds (MATLAB) was also provided by the authors.

2.6. Experiments

Several experiments were carried out to identify the most critical steps and relevant model parameters of the computational pipeline, as well as the similarity between simulations and observations. First, we assessed the accuracy of the fetal brain segmentations provided by the modified dHCP structural pipeline, comparing them with ground-truth

Table 2
Comparison between ground-truth and automatic segmentations.

	Dice Coefficient	Hausdorff Distance (mm)	Volume Similarity
Grey matter	0.78 ± 0.05	6.49 ± 1.06	0.96 ± 0.03
White matter	0.95 ± 0.01	8.80 ± 1.80	0.99 ± 0.01

manual annotations. Second, a sensitivity analysis on the simulations was performed, running the model with six different initial global cortical thicknesses (H_i), ranging from 0.74 mm to 5.96 mm in a subset of 8 fetal meshes (4 VM; 2 of early and 2 of late-onset; 4 controls; 2 of early and 2 of late-onset). Values were chosen as in [66], of which 0.74 mm and 5.96 mm were assumed to be abnormal H_i values. An additional simulation was run for each subject with the global cortical thickness derived from its corresponding patient-specific MRI (i.e., average over the whole brain). The effect of regional growth was then assessed, using a cortical parcellation (using the DrawEM tool [39, 40]) to specify a different growth for each region in the biomechanical model.

3. Results

3.1. Data preprocessing

Figure 2 displays a visual comparison between ground-truth and automatic segmentation results provided by the modified dHCP pipeline. Beyond the central region in white matter (not relevant in our study) some discrepancies were found in regions with larger curvature. Quantitative results are shown in Table 2. An average Dice of 0.78 ± 0.05, HD of 6.49 ± 1.06 and VS of 0.96 ± 0.03 were obtained for grey matter, and of 0.95 ± 0.01, 8.80 ± 1.80 and 0.99 ± 0.01, respectively, for white matter and ventricles. Snapshots of all fetal and neonatal meshes of grey matter used in this study are included in Appendix A. Two of the 31 initial cases were discarded for the final cohort because the segmentation step did not provide grey matter labels that could be used to build finite-element meshes (i.e., not continuous tissue requiring excessive manual intervention).

Figure 2 also provides a visual example of a cortical thickness map obtained with the Pyezzi python library. Cortical thickness in fetal MRI ranged from 1.20 mm to 1.78 mm, with mean value and standard deviation of the mean 1.53 ± 0.16 mm and within-subject mean standard deviation of 0.45 mm. The cortical thickness measured in neonatal MRI was 1.32 ± 0.17 mm.

Sets of fetal, neonatal and simulated meshes are displayed in Figures 7, 8 and 9, respectively.

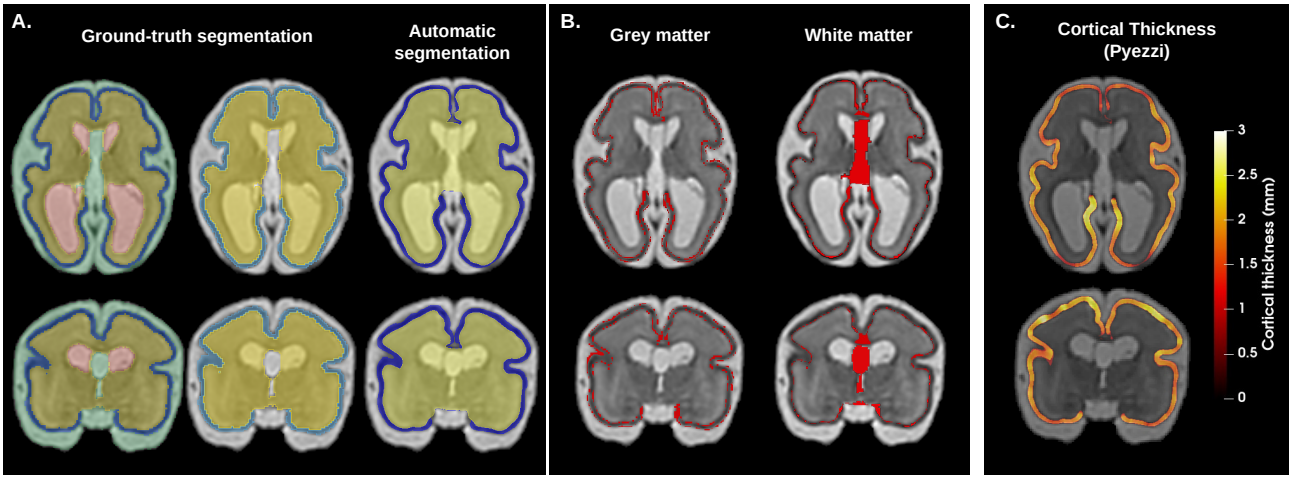

Figure 2: Comparison of ground-truth and automatic segmentations. (A) Axial and coronal views of ground-truth segmentations (all labels and only grey and white matter combined with ventricles) and automatic segmentations. (B) Differences (red) in grey (left) and white (right) matter. (C) Cortical thickness estimated from magnetic resonance images.

3.2. In-silico simulations

3.2.1. Varying global cortical thickness in brain simulations

The effect of having distinct initial global cortical thickness in brain simulations can be seen in Figure 3. Mean curvatures were plotted versus H_i (Figure 3.A), quantitatively showing the decrease in curvature in all meshes when increasing cortical thickness. Both mean curvature and depth potential function mapped onto cortical surfaces and spheres (Figure 3.B) clearly displayed how low values of H_i created overly convoluted cortex, while with high values gyri became fewer and wider. In terms of folding bands, SPANGY results (Figure 3.D) showed that the power spectrum of curvature was mostly of band 6 with the smaller cortical thickness value (i.e., $H_i = 0.74$ mm), mainly creating folding patterns similar to tertiary folds. As cortical thickness increased, the power in bands 5 and 6 also progressively rose, while that of band 4 decreased. Power spectrum maps plotted on the cortical surfaces (Figure 3.E) illustrate this scenario, with a greater presence of bands 5 (orange) and 6 (red) at higher values of H_i, where the nature of the folding was of first and second order.

3.2.2. Global vs regional growth in brain simulations

Results of this experiment are shown in Figure 4. With the implemented regional growth, the simulated mesh presented slightly increased volume in the parietal and occipital areas, although still far from the global shape of the real neonatal cortex (see Figure 4.A). The standard deviation between the coordinates of the vertices of the simulated and neonatal meshes was mapped on an inflated surface, as can be observed in Figure 4.B). It depicts how regional growth reduced the differences between simulations and observations in the parietal area. Box plots of global metrics also showed an increase in volume and surface area of regional simulations compared to baseline (Figure 4.C).

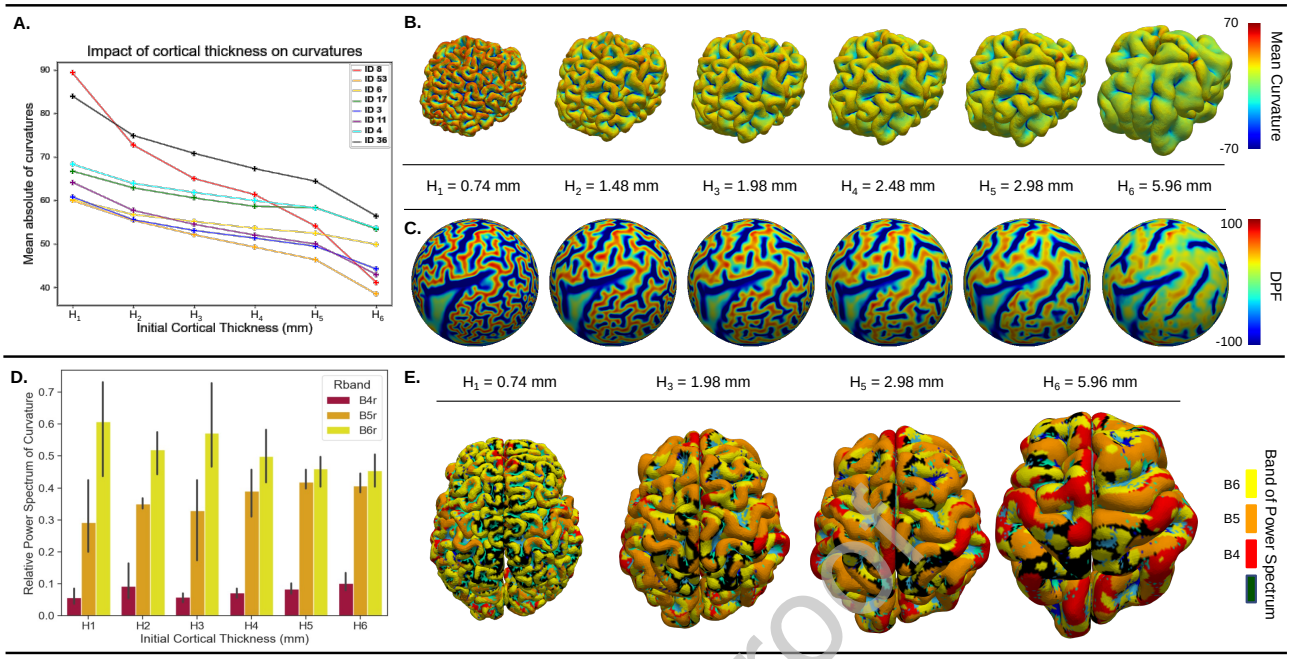

Figure 3: Impact of varying initial cortical thickness on simulated meshes. (A) Plot of mean absolute value of curvature of each mesh and level i of cortical thickness (H_i) ranging from 1 to 6. (B) Simulated cortical morphologies with curvature maps and (C) spheres coloured by the depth potential function (DPF) obtained with each initial cortical thickness. (D) Relative power spectrum of curvature in bands B4-B6 displayed as a bar plot and (E) onto cortical surfaces for four of the implemented H_i.

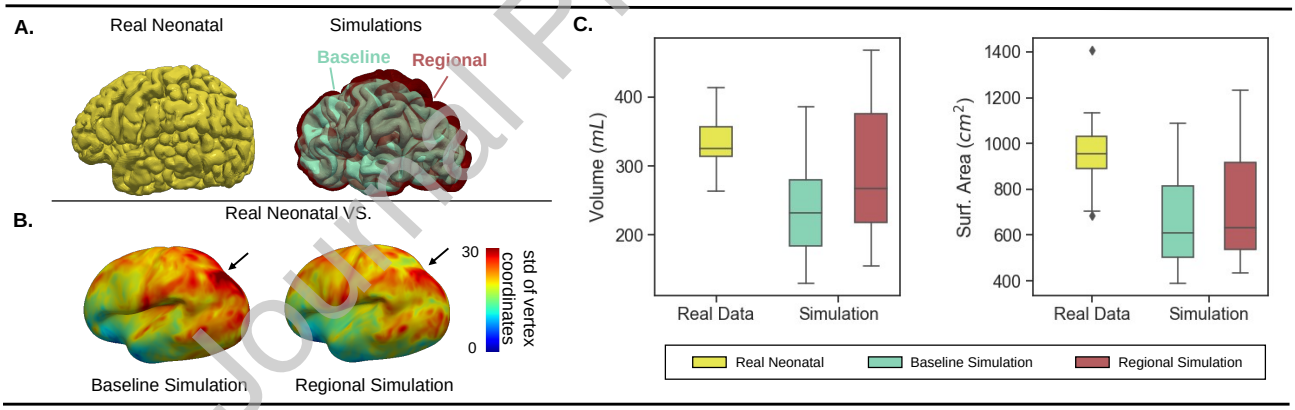

Figure 4: Comparison between simulations with global and regional growth. (A) For one subject, neonatal real cortex and both overlapped global and regional growth simulations. (B) Standard deviation of the vertex coordinates between neonatal and brain simulations plotted onto an inflated surface. Arrows point to the parietal region. (C) Box plots of volume and surface area for each group of meshes.

3.2.3. Neonatal data vs brain simulations

A comparison between neonatal real data and simulations is shown in Figure 5. Cortical surfaces and curvature maps of fetal, neonatal and simulations are displayed for two subjects (Figure 5.A): 1) a ventriculomegaly condition, with fetal MRI acquired at GA 28 (early onset); and 2) a control case, with fetal imaging available at GA 32 (late onset). Although the nature of the folding patterns was reproduced by the biomechanical model, there were notable

differences when comparing simulated to real neonatal meshes. The sagittal view of the cortices revealed a lack of similarity in their overall shape, especially in the parietal region, which more closely resembled that observed in the fetal meshes. Regarding the time (onset) at which fetal MRIs were acquired, simulations starting at advanced GA were more comparable to their corresponding real neonatal meshes. Conversely, simulations of meshes starting from GA 26-28 had a lower match with their corresponding neonatal real data. Fetal brains at early GA, apart from being smaller in size than neonatal ones, only presented the central and lateral sulcus (Sylvian fissure); the absence of more complete structural information resulted in simulations with higher variability. The identification of sulci was visually performed on the DPF maps plotted onto spheres. The Sylvian fissure, central sulcus, post-central sulcus and superior temporal sulcus were identified in all six meshes, thus revealing the ability of simulations to reproduce these patterns.

Figure 5.B shows the atlases of each group of meshes (i.e., fetal, simulation, neonatal), coloured by the depth potential function estimation. It can be seen that the average cortical surface of simulations have created several gyri (red colours in the figure) from the fetal stage, but not as many as observed in the neonatal atlas. Box plots of global metrics are in displayed in Figure5.C to compare fetal, simulation and neonatal brains. The simulations underestimated the surface area, volume and 3D-GI observed in neonatal meshes, by a 30.9%, 26.9% and 14.4%, respectively.

3.2.4. Controls vs ventriculomegaly cases

Figure 6 displays differences between control and VM cases, for both simulations and real data. Surface area and volume were underestimated by simulations when compared to values of neonatal meshes. The increase in fetal surface area and volume in the simulations was of 64% and 42%, respectively, whilst real neonatal meshes had an increase of 75% and 58%. No significant differences were observed in mean surface values between controls and VM, but controls presented lower volume (6%) than VM in both simulated and real meshes ($p < 0.05$). 3D-GI was lower in simulations than in real neonatal meshes; values for controls (simulations: 2.68 ± 0.31, neonatal: 3.20 ± 0.32) were higher than for VM (2.63 ± 0.27, 2.99 ± 0.37).

Results in depth potential function and mean curvature were similar for both groups: fetal cases, 12.75 ± 6.64 (controls) and 11.11 ± 4.53 (VM); neonatal cases 33.29 ± 4.62 (controls) and 33.62 ± 4.37 (VM); and simulations, 45.12 ± 6.57 (controls) and 42.81 ± 7.65 (VM). Statistically significant differences ($p < 0.05$) were obtained between simulations and neonatal data but not between VM and controls. In addition, fetal meshes showed bigger mean and dispersion of the KL divergence, i.e., more isotropy in their surface orientation: controls: $6.34 \pm 4.57xE-03$; VM, $4.96 \pm 5.16xE-03$. Simulations presented larger KL divergence values than neonatal meshes (26% in controls and 35% in VM), which suggested less anisotropy in their fold orientation.

SPANGY results are shown in Figure 6.B. No significant differences were observed between controls and VM in none of the three groups (fetal, neonatal, simulations). Fetal meshes presented higher values of relative folding

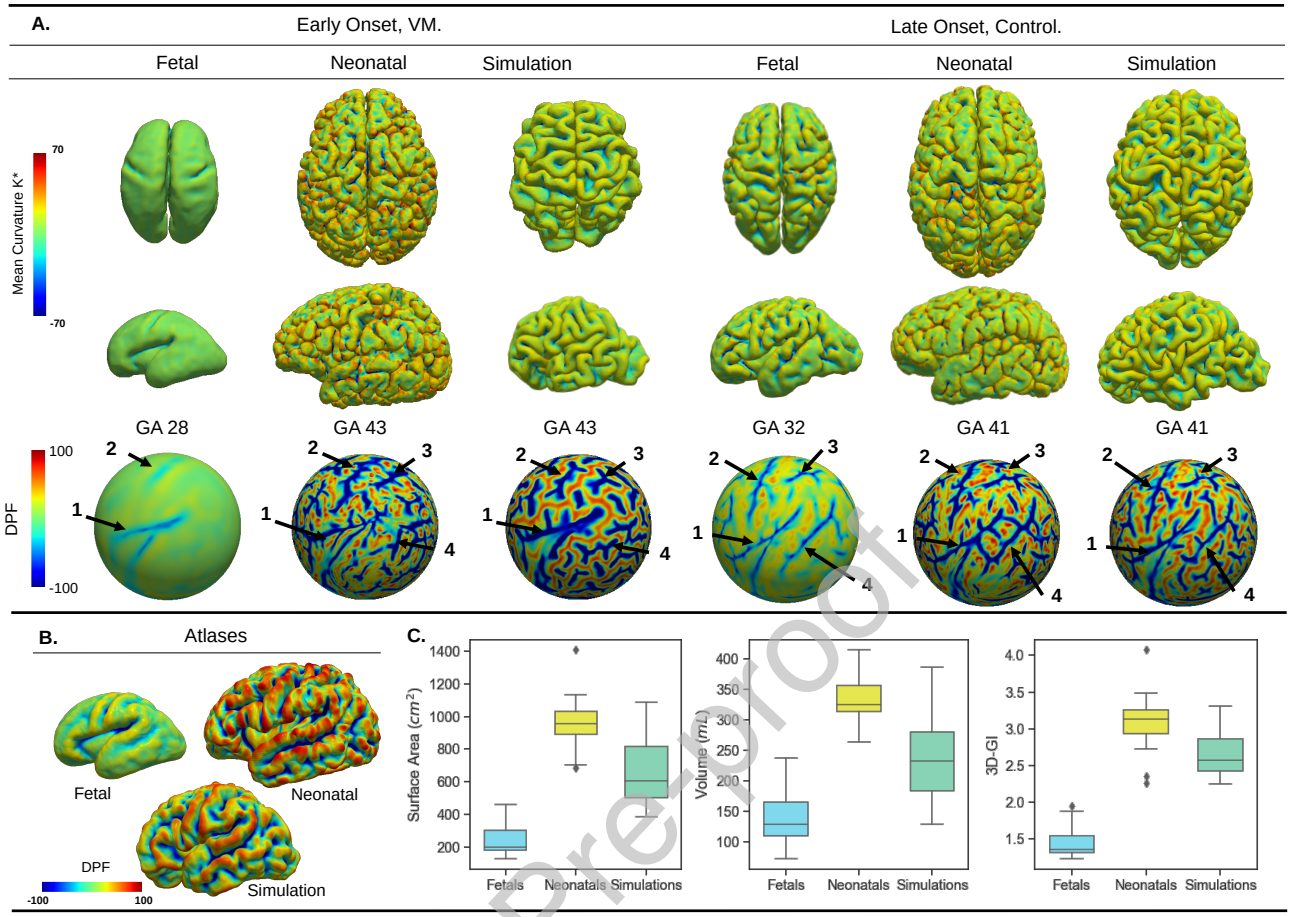

Figure 5: (A) Cortical morphologies and curvature maps of fetal and neonatal meshes of two subjects (a ventriculomegaly, VM, fetal brain at early gestation and a control one of late onset), together with the resulting brain simulations. Depth potential function (DPF) maps are mapped onto spheres with arrows pointing at the following: 1 = Sylvian fissure; 2 = Central sulcus; 3 = Post-Central sulcus; 4 = Superior Temporal sulcus. (B) Atlases of real fetal and neonatal and simulated meshes. (C) Global metrics of surface area, volume and 3D gyrification index (3D-GI) for the whole cohort.

power in band 4 (0.154 ± 0.057) than neonatal ones (0.048 ± 0.01) and simulations (0.079 ± 0.019). For neonatal real data, power spectrum in band 6 (0.628 ± 0.023) roughly doubled the power in band 5 (0.285 ± 0.025), while for simulations they were of 0.440 ± 0.081 in band 5 and 0.431 ± 0.111 in band 6. Atlases and inflated surfaces with DPF (Figure 6.C), qualitatively showed how, although minor discrepancies in folding were present between controls and VM, major differences in size, shape and folding were prominent between groups. Overall, results showed that the differences between simulations and real data were much larger than those observed between pathological and healthy conditions.

3.2.5. Computational times

Table 3 shows a breakdown of the tasks performed at each step of the pipeline along with an estimate of the computational time required to complete them. Segmentation with the dHCP structural pipeline took 15-20' for each

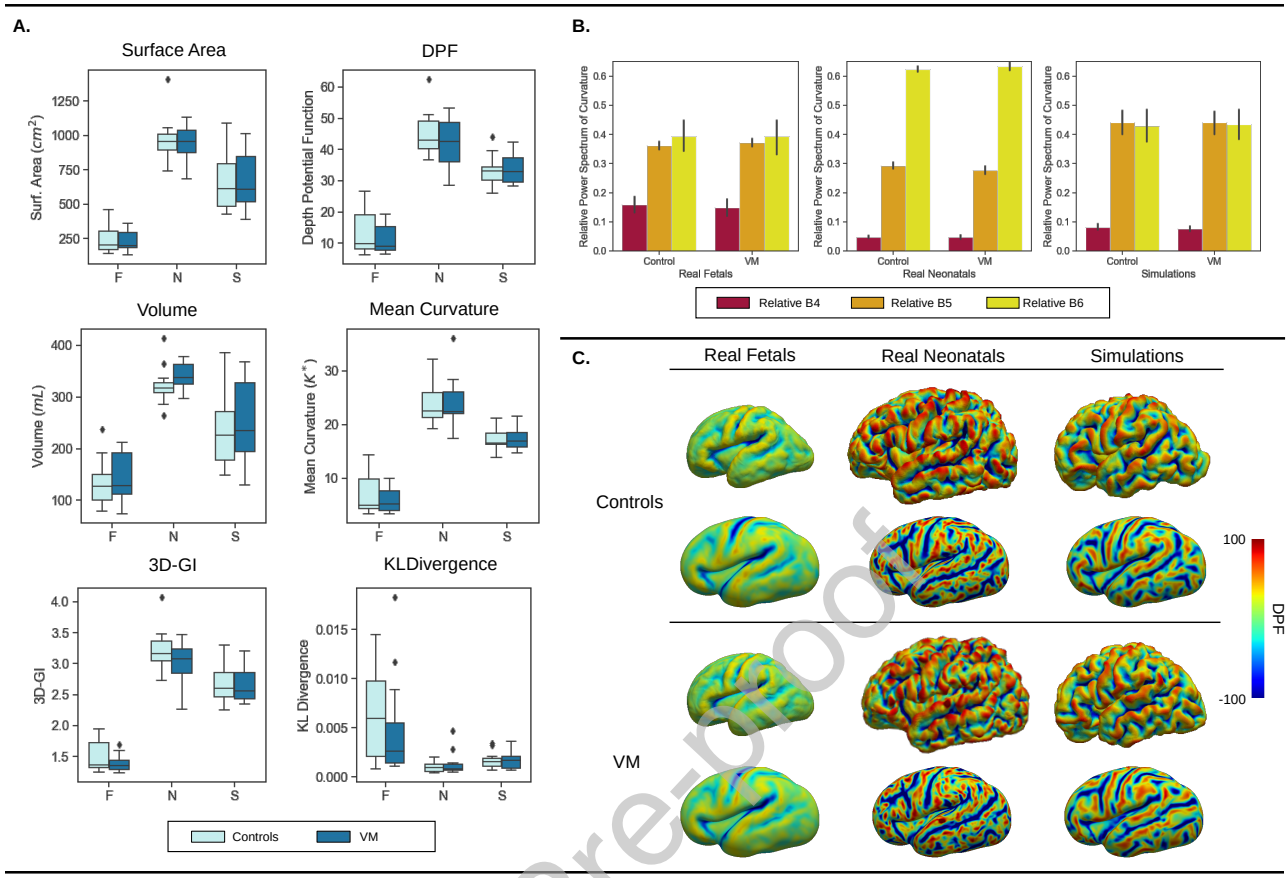

Figure 6: Comparison of real data and simulations for control and ventriculomegaly (VM) cases. (A) Box plots for global metrics and mean values of depth potential function (DPF), mean curvature and Kullback-Leibler (KL) divergence. (B) Bar plots of relative power spectrum of curvature in folding bands. (C) Atlases of cortical surfaces for each group of meshes (control and VM, simulations (S), real fetal (F) and neonatal (N)), coloured by DPF distribution. Below each atlas, inflated versions of the surfaces are included.

MRI dataset. Mesh processing took around 20-30' but it could vary depending on the nature of meshes, since this step was highly manual. The computational model was the longest process, in particular when the solver did not converge the first time it was run. In that case, in an iterative manner the mesh was re-processed (by repairing the problematic area or re-meshing the whole mesh), the volumetric mesh was generated again and the model was re-run. The calculation of the evaluation metrics required different times. For instance, SPANGY is time-consuming because it requires to solve a generalized eigenvalue problem with thousand of eigenvectors in a very large dimension.

Table 3
Computational time required to run the whole pipeline.

Pipeline Stage	Task (software)	Computational time (min)
Segmentation	Segmentation (dHCP structural pipeline)	15-20'
Mesh Processing	Mesh Processing (Meshmixer)	20-30'
	Volumetric mesh generation (Netgen)	3-5'
Computational Model	C++ Solver (HPC Cluster)	25-35 h
Evaluation metrics	Global metrics (Slam, Python)	<1'
	Mean curvature (Slam, Python)	5-8'
	SPANGY (Matlab)	15-30h
	Depth potential function (Slam, Python)	3-5'
	Folds orientation (Matlab)	20-30'
	aMSM	10-15'

4. Discussion

Personalised computational models are progressively being more used in medical fields such as cardiology [45], to support diagnosis [14], therapy optimisation and risk prediction [42]. Together with statistical (e.g., machine learning) models, they are the foundations of digital twins for improved patient-specific clinical decisions and precision medicine [13]. However, mechanical models of brain development are not that mature yet, basically been tested on synthetic or idealised geometries due to the difficulties of obtaining longitudinal imaging data. However, recent advances in imaging acquisition and processing techniques are leading to better quality images of the fetal and neonatal brain. In this work, we present a computational pipeline, based on open-source tools, that allowed to successfully process fetal MR images of 29 subjects, building patient-specific meshes to simulate brain growth/folding, and comparing the resulting simulations with neonatal data from the same subjects with several global and local metrics in a common reference space. The different steps in the pipeline for geometrical model building and the brain mechanical modelling influenced the final simulation results and its comparison with neonatal data, as described in the following.

4.1. Geometrical model building

4.1.1. Brain segmentation

Brain segmentation was the initial step of the pipeline since fetal MRI 3D reconstruction was already performed in the standard imaging protocol in the hospital. Inaccuracies to reconstruct fetal MR images would obviously affect the whole modelling pipeline; it is then necessary to apply motion correction algorithms (see [6] for options) to provide high-resolution 3D data to process.

Patient-specific brain modelling of several cases requires the automatisation of 3D fetal brain MR data segmentation. In our work, we were able to compare brain tissue segmentations provided by the modified dHCP pipeline with manual labels in 13 fetal MR images. Overall, automatically obtained grey matter labels were similar to the ground-truth after visual inspection of the results (see Figure 2, with more differences in the area between the hemispheres and systematically over-estimating sulcal depth. The estimated quantitative metrics (e.g., Dice) were good enough (0.78, above inter-rater variability recently measured in [46]), considering the complexity of cortical morphology. However, two cases (out of 31) were discarded due to inaccurate GM segmentation that would require almost fully manual labelling. Improved fetal brain segmentation techniques, using deep learning techniques, are already appearing (e.g., [36]) thanks to the availability of Open Access data in initiatives such as the Fetal Tissue Annotation (FETA) challenge [46][13]. Regarding neonatal brain segmentation, we made use of the standard dHCP pipeline [40] (Dice of around 0.80 for cortical GM, reported in [39]) but its accuracy in our data could not be quantified due to the lack of ground-truth data at this stage.

[13] https://feta-2021.grand-challenge.org/

4.1.2. Cortical thickness estimation

In the implemented brain mechanical model, the initial cortical thickness (width of grey matter layer) is a key parameter for the simulated folding [66]. Cortical thickness estimation directly depends on the brain segmentation accuracy. Using a well-known tissue thickness method [71], the cortical thickness values for fetal MRI (average of 1.53 ± 0.16 mm) were larger than the ones reported in [9] (average of 1.05 mm) but within the range of the ones published in Vasung et al. [63] (1-2 mm from GA 26 until 42). On the other hand, we found cortical thickness estimated in neonatal data less reliable. In a counter-intuitive way, the average value of cortical thickness was lower in neonatal than in fetal data. Neonatal cortical thickness was estimated from the dHCP-based segmentations, from which values of 1.04 mm at 36 weeks to 1.10 mm at 44 weeks have been reported [40], in concordance with our results. The main reason for this discrepancy was the topological differences in GM segmentations in the two stages, with neonatal segmentations being too thin and discontinuous comparing to fetal ones, having a large influence on cortical thickness values.

4.1.3. Meshing

Building patient-specific meshes of human organs with complex morphologies is one of the main bottlenecks that has prevented a more widespread clinical translation of computational models, due to the difficulties on automatising the process. Tetrahedral meshes were chosen to build patient-specific brain meshes since they usually can better discretise complex geometries than hexahedral representations. Still, the building of 29 patient-specific brain meshes was a labour-intensive process that should be better streamlined in the future. Mechanically evolving a fetal, relatively smooth, brain into the highly convoluted cortical surface post-natally is a numerical problem pushing FEM techniques to the limit. For instance, large deformations may be needed but they may lead to negative Jacobian or overlapping elements impeding finding correct solutions. Sophisticated meshing and solver methodologies are required, often asking for manual intervention in an iterative framework. In our experiments, 10 cases out of 29 needed several re-meshing iterations (i.e., removing or smoothing elements, correcting topological defects such as handles or holes) to ensure convergence of the solutions. The contact penalty force implemented in [59] was key to avoid non-negative Jacobian mesh elements through simulation time-steps. Meshless techniques such as the ones based on smooth particle hydrodynamics, already successfully applied for electromechanical simulations of the heart [37], or based on the material point method to study live human brain dynamics [19], should be explored for brain development modelling since they are suitable when meshing is challenging.

4.2. Brain mechanical modelling

Initially, the available open-source brain mechanics solver was adapted to have as input any fetal brain geometrical mesh, at any initial GA and delivery week, since several routines were hard-coded to only work on particular idealised

geometries. Starting from patient-specific fetal brain geometries, the model was able to reproduce the convoluted nature of brain folding patterns in neonatal stages described in [59, 20]. Spherical representations of metrics (e.g., DPF in Figure 5) were effective to identify the resemblance of certain sulcal patterns (e.g., central and post-central sulcus, 2 and 3 in Figure 5, respectively) between neonatal simulations and observations, even in cases starting from an early GA fetal mesh. It is remarkable the stability of the central and temporal sulci through the simulation process, as it was earlier demonstrated in spheres [34], likely due to their presence in fetal meshes (range between 26 to 34 GA). Nevertheless, it is evident that the simulated meshes still present large differences with real neonatal data in terms of global shape and folding patterns (see results in Figure 5 and Figure 6). Mechanical simulations consistently generated smaller (as seen by the surface area and volume metrics) and less convoluted (from 3D-GI and curvature metrics) brains that neonatal real ones. The detailed characterisation of folds with SPANGY, DPF and orientation-based metrics showed that simulations created, compared to neonatal real patterns: 1) less convex folds in average and with a smaller range of different values (from DPF); 2) less uniform (i.e., isotropic) fold orientation (from KL divergence); and 3) an insufficient percentage of secondary folds (see orange bars in Figure 6 corresponding to B5), slightly overestimating primary folds. The more isotropic orientation of the folds in the simulations was due to the model assumption of uniform and isotropic growth across the entire grey matter geometry, which is an over-simplification of brain growth dynamics during fetal brain development. Comparing simulated neonatal brains of controls and ventriculomegaly cases, we observed the same subtle differences than in real data in all metrics: slightly less convoluted brain (from 3D-GI) and reduced volumes in ventriculomegaly cases, in agreement with literature [56, 33, 7]. To complement the evaluation of the simulations, future studies will also include the computation and analysis of the sulcal depth, sulci identification and number of folds.

It is important to point out the relevance of the initial fetal brain gestational age, as can be seen in Figure 5: with initial smoother meshes (i.e., earlier GA such as in Figure 5.A), the brain mechanical model generates simulated neonatal brains further from data than with initial meshes where more folds are present (i.e., later fetal GA, such as in Figure 5.B). This is in agreement with conclusions found in the literature [30, 49, 17], stating that first order folds are thought to be regulated by genetic and cellular pre-patterning processes. These were not included in our experiments since initial fetal brain meshes in our study were from 26 weeks on, with primary folds already formed. Recent pioneering work on multi-scale modelling of brain development [72], including cellular dynamics, has the potential to better simulate the generation of folds that have not appeared yet. Additionally, it would be interesting to incorporate axonal tension forces to the current model of Tallinen et al. [58, 59] since it is only based on the differential growth between cortical and white matter regions. As seen in [20], although it has been demonstrated that axonal tension does not drive gyrification, it does have a relevant role in the modulation of folding patterns.

Two additional parameters were important to obtain different brain simulation patterns: cortical thickness and

brain growth characteristics. When modifying the initial global cortical thickness, the resulting simulations were in agreement with literature [17, 66], with a thinner cortex leading to more folded brains and vice versa (such as in polymicrogyria and lissencephalic brains, respectively). In our sensitivity analysis, imposing an initial cortical thickness of 1.48 mm or 1.98 mm (H_2 and H_3 in Figure 3) provided the closer simulations to neonatal data. However, we finally tailored the initial global cortical thickness for each simulation to the one extracted from the MRI of each individual, further personalising the model. In this context, it is also worth mentioning that differences in the order of the resolution of the acquired magnetic resonance images (0.5 mm) should not be relevant. In the future, different cortical thickness values will be imposed locally to different regions based on MRI estimations, which should lead to less homogeneous and more realistic behaviour of the simulated folding patterns.

For simplicity, cortical growth was initially assumed uniform and isotropic in the initial experiments. However, previous studies have demonstrated inter-hemisphere gyrification differences [48] and non-homogeneous shape changes between fetal and neonatal cortical surfaces [21]. A simple implementation of regional growth was then implemented, showing qualitative and quantitative improvements in certain areas such as the parietal region. Refined spatio-temporal local growth patterns based on prior observations (e.g., from Garcia et al. [21]), already partially tested on atlas fetal brains [65], will improve the realism of the presented brain simulations. In parallel, anisotropic growth could be incorporated, as in [64], dependent on the mean curvature of the cortex to achieve preferential growth in either gyri or sulci. Local constraints based on the particular characteristics of individual sulci and related cytoarchitecture, in particular the primary folds (e.g., central sulcus), would help to better control the folding pattern evolution in the simulations. Additionally, the equations of the biomechanical model accounted for a stress-independent growth, with values being imposed throughout the simulation. For more realistic simulations, the model must be modified to allow for biomechanical feedback, so that growth is readjusted according to the stress fields generated at each point in the process.

Material properties of both grey and white matter were defined globally by the bulk and shear modulus. However, there is evidence that they vary significantly not only across regions of the brain [11], but also throughout the fetal development, when the brain constantly adapts to new functional demands. A better characterization of brain tissue mechanical properties is becoming possible with recent advanced experimental set-ups [10] and should definitively be integrated into the existing brain development models. Sensitivity analysis studies should then be carried out to assess the influence of material properties on the simulation results.

5. Conclusions

Computational models of brain development are arguably in its infancy, comparing to the ones in other human organs such as the heart. One of the main causes is the absence of validation studies confronting simulation results with

observations, due to the difficulty of having longitudinal brain data from the same subject. More multi-disciplinary efforts between data scientists, modellers and clinicians would also be beneficial for improving the realism of existing simulations. In this work we have presented a complete pipeline for creating and validating patient-specific mechanical models of brain development, which has been applied to 29 fetal brain MRI data. Simulations of neonatal brains remarkably mimicked folding patterns observed in MR images. However, the developed pipeline allowed to quantify important differences between model results and observations at different time-points or subjects, both globally and locally, with the employed metrics and the building of a common reference system. In consequence, some of these metrics could be used for model parameter optimisation within data assimilation processes such as for determining the optimal cortical growth in each region to better match neonatal data. The different open-source tools used in the presented pipeline also facilitate joint multi-institutional efforts, necessary to bring the field of brain mechanical modelling forward. Initiatives such as the dHCP[14], releasing tools and data for fetal and neonatal imaging research, will soon allow the creation of benchmark studies to compare models based on different hypothesis (i.e., axonal tension, differential growth, stress-dependent growth) and integrate them, together with other statistical or phenomenological approaches such as disease progression models [2]. Brain mechanical model researchers should then follow the example of neuroimaging researchers, pioneers in Open Science, and jointly work in multi-disciplinary teams with neurologists to better understand the wonders of brain development.

CRediT authorship contribution statement

Mireia AlenyÃă: Conceptualisation of the study, methodology, implementation of experiments, writing manuscript. **Xiaoyu Wang:** Implementation of mechanical model and evaluation metrics. **Julien LefÃÍvre:** Conceptualisation of the study, evaluation metrics, manuscript revision. **Guillaume Auzias:** Conceptualisation of the study, evaluation metrics, manuscript revision. **Benjamin Fouquet:** Implementation of mechanical model. **Elisenda Eixarch:** Data provider, conceptualisation of the study, clinical feedback. **FranÃğois Rousseau:** Conceptualisation of the study, mechanical model, evaluation metrics, manuscript revision. **Oscar Camara:** Conceptualisation of the study, mechanical model, evaluation metrics, manuscript writing.

A. Meshes of the whole cohort

[14] http://www.developingconnectome.org/project/

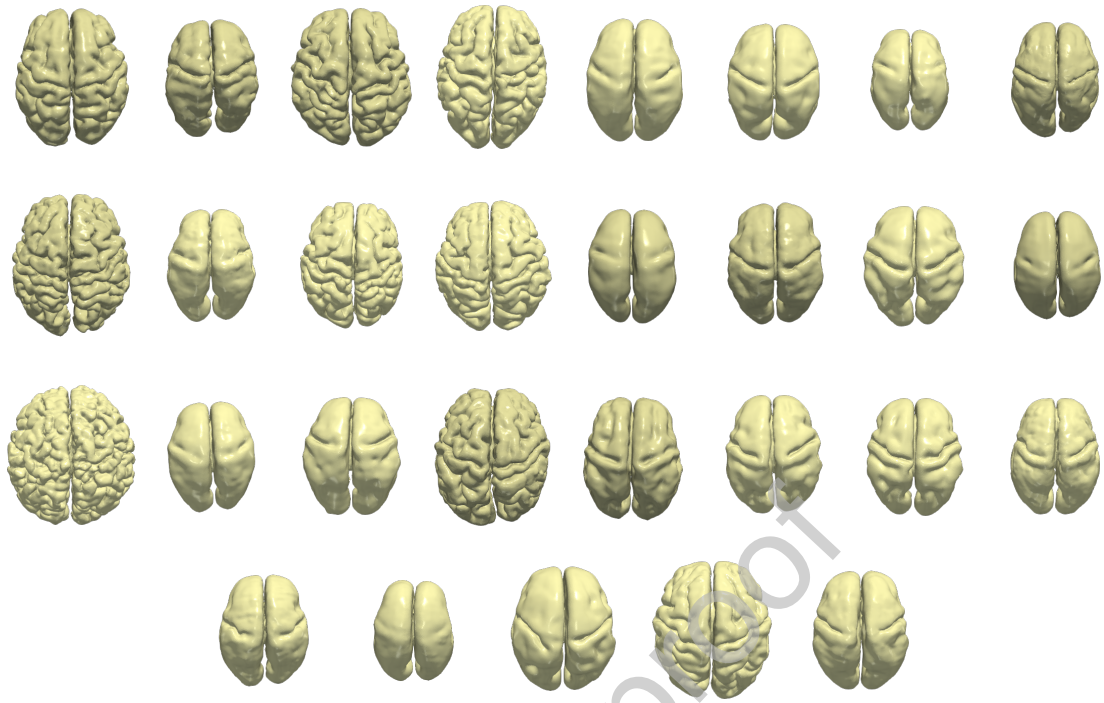

Figure 7: Fetal grey matter geometries of the entire cohort. The 29 meshes were extracted from the magnetic resonance images and set as starting point of the biomechanical model. Gestational age ranged from 26.3 to 34.7 weeks. More information on the dataset can be found in Table 1.

References

[1] Armstrong, E., Schleicher, A., Omran, H., Curtis, M., Zilles, K., 1995. The Ontogeny of Human Gyrification. Cerebral Cortex 5, 56–63.

[2] Banus, J., Lorenzi, M., Camara, O., Sermesant, M., 2021. Biophysics-based statistical learning: Application to heart and brain interactions. Medical Image Analysis 72, 102089.

[3] Barnette, A.R., Neil, J.J., Kroenke, C.D., Griffith, J.L., Epstein, A.A., Bayly, P.V., Knutsen, A.K., Inder, T.E., 2009. Characterization of Brain Development in the Ferret via MRI. Pediatric Research 2009 66:1 66, 80–84.

[4] Bayly, P.V., Clayton, E.H., Genin, G.M., 2012. Quantitative imaging methods for the development and validation of brain biomechanics models.

[5] Bayly, P.V., Okamoto, R.J., Xu, G., Shi, Y., Taber, L.A., 2013. A cortical folding model incorporating stress-dependent growth explains gyral wavelengths and stress patterns in the developing brain. Physical Biology .

[6] Benkarim, O., Sanroma, G., Zimmer, V., Muñoz-Moreno, E., Hahner, N., Eixarch, E., Camara, O., González Ballester, M., Piella, G., 2017. Toward the automatic quantification of in utero brain development in 3D structural MRI: A review. Human Brain Mapping 38.

[7] Benkarim, O.M.e.a., 2018. Cortical folding alterations in fetuses with isolated non-severe ventriculomegaly. NeuroImage: Clinical .

[8] Boucher, M., Whitesides, S., Evans, A., 2009. Depth potential function for folding pattern representation, registration and analysis. Medical Image Analysis 13, 203–214.

[9] Bozek, J., Makropoulos, A., Schuh, A., Fitzgibbon, S., Wright, R., Glasser, M.F., Coalson, T.S., O'Muircheartaigh, J., Hutter, J., Price, A.N., Cordero-Grande, L., Teixeira, R.P.A., Hughes, E., Tusor, N., Baruteau, K.P., Rutherford, M.A., Edwards, A.D., Hajnal, J.V., Smith, S.M., Rueckert, D., Jenkinson, M., Robinson, E.C., 2018. Construction of a neonatal cortical surface atlas using multimodal surface matching in

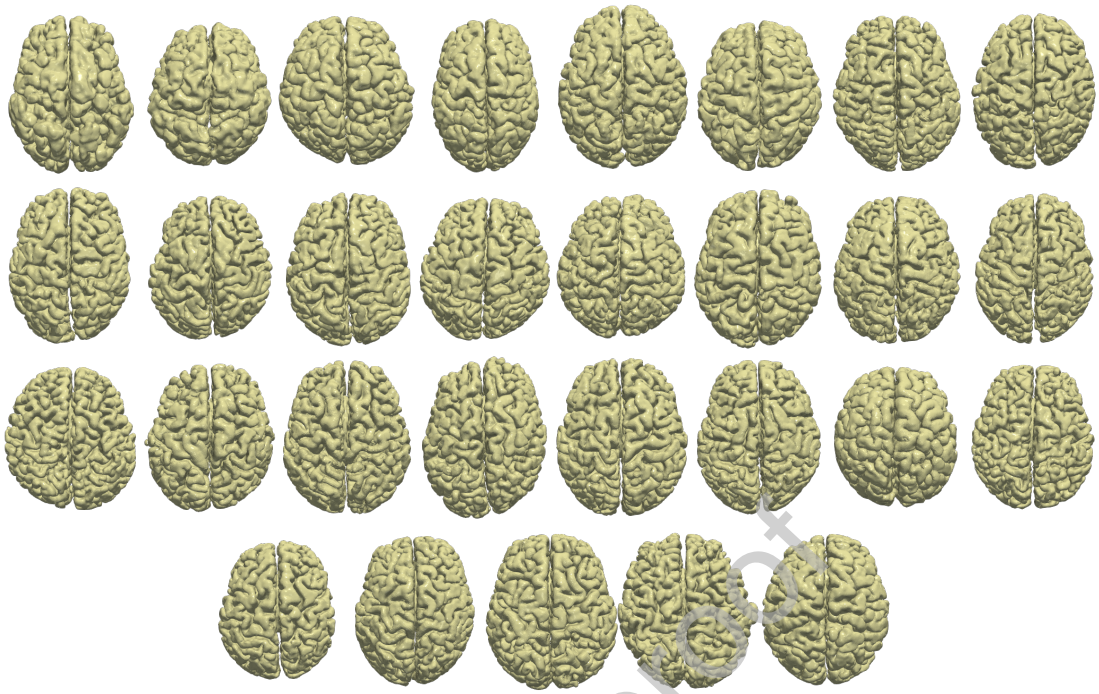

Figure 8: Neonatal grey matter geometries of the whole cohort. The 29 meshes were extracted from magnetic resonance images and used to assess simulation results. Gestational age ranged from 39.9 to 47.6 weeks. More information on the dataset can be found in Table 1.

the developing human connectome project. NeuroImage 179, 11–29.

[10] Budday, S., Ovaert, T.C., Holzapfel, G.A., Steinmann, P., Kuhl, E., 2019. Fifty Shades of Brain: A Review on the Mechanical Testing and Modeling of Brain Tissue. Archives of Computational Methods in Engineering 2019 27:4 27, 1187–1230.

[11] Budday, S., Steinmann, P., Kuhl, E., 2014. The role of mechanics during brain development. Journal of the Mechanics and Physics of Solids 72, 75–92.

[12] Clark, W.E.L.G., 1945. Deformation patterns in the cerebral cortex. Printed at the Oxford University Press by John Johnson.

[13] Corral-Acero, J., Margara, F., Marciniak, M., Rodero, C., Loncaric, F., Feng, Y., Gilbert, A., Fernandes, J.F., Bukhari, H.A., Wajdan, A., Martinez, M.V., Santos, M.S., Shamohammdi, M., Luo, H., Westphal, P., Leeson, P., DiAchille, P., Gurev, V., Mayr, M., Geris, L., Pathmanathan, P., Morrison, T., Cornelussen, R., Prinzen, F., Delhaas, T., Doltra, A., Sitges, M., Vigmond, E.J., Zacur, E., Grau, V., Rodriguez, B., Remme, E.W., Niederer, S., Mortier, P., McLeod, K., Potse, M., Pueyo, E., Bueno-Orovio, A., Lamata, P., 2020. The âĂŸDigital Twin' to enable the vision of precision cardiology. European Heart Journal 41, 4556–4564.

[14] Doste, R., Sebastian, R., Gomez, J.F., Soto-Iglesias, D., Alcaine, A., Mont, L., Berruezo, A., Penela, D., Camara, O., 2020. In silico pace-mapping: prediction of left vs. right outflow tract origin in idiopathic ventricular arrhythmias with patient-specific electrophysiological simulations. EP Europace 22, 1419–1430.

[15] Dubois, J., Benders, M., Cachia, A., Lazeyras, F., Ha-Vinh Leuchter, R., Sizonenko, S.V., Borradori-Tolsa, C., Mangin, J.F., HÃijppi, P.S., 2007. Mapping the Early Cortical Folding Process in the Preterm Newborn Brain. Cerebral Cortex 18, 1444–1454.

[16] Ericson, C., 2005. Real-Time Collision Detection.

[17] Fernández, V., LlinaresâĂŘBenadero, C., Borrell, V., 2016. Cerebral cortex expansion and folding: what have we learned? The EMBO Journal 35, 1021.

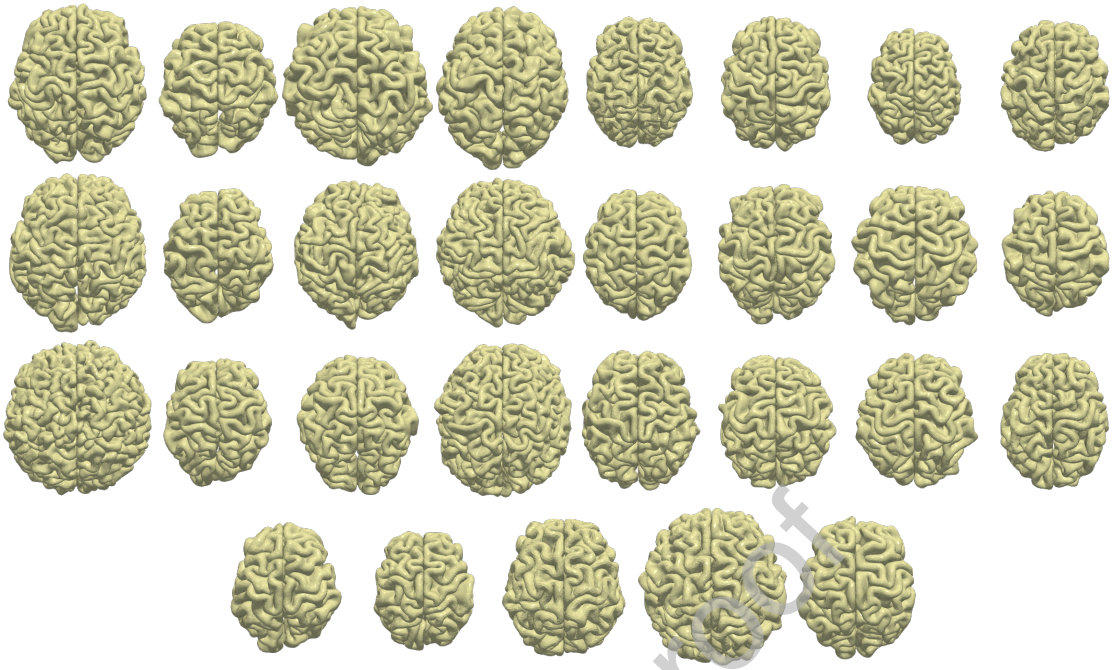

Figure 9: Simulated grey matter geometries at corresponding neonatal gestational age. The 29 meshes were obtained using the biomechanical brain growth model with the fetal geometries of Figure 7 as a starting point.

[18] Foubet, O., Trejo, M., Toro, R., 2019. Mechanical morphogenesis and the development of neocortical organisation. Cortex 118, 315–326.

[19] Ganpule, S., Daphalapurkar, N.P., Ramesh, K.T., Knutsen, A.K., Pham, D.L., Bayly, P.V., Prince, J.L., 2017. A Three-Dimensional Computational Human Head Model That Captures Live Human Brain Dynamics. Journal of Neurotrauma .

[20] Garcia, K.E., Kroenke, C.D., Bayly, P.V., 2018a. Mechanics of cortical folding: Stress, growth and stability. Philosophical Transactions of the Royal Society B: Biological Sciences 373.

[21] Garcia, K.E., Robinson, E.C., Alexopoulos, D., Dierker, D.L., Glasser, M.F., Coalson, T.S., Ortinau, C.M., Rueckert, D., Taber, L.A., Van Essen, D.C., Rogers, C.E., Smyser, C.D., Bayly, P.V., 2018b. Dynamic patterns of cortical expansion during folding of the preterm human brain. Proceedings of the National Academy of Sciences of the United States of America .

[22] Germanaud, D., Lefèvre, J., Toro, R., Fischer, C., Dubois, J., Hertz-Pannier, L., Mangin, J.F., 2012. Larger is twistier: Spectral analysis of gyrification (SPANGY) applied to adult brain size polymorphism. NeuroImage .

[23] Gholipour, A., Rollins, C.K., Velasco-Annis, C., Ouaalam, A., Akhondi-Asl, A., Afacan, O., Ortinau, C.M., Clancy, S., Limperopoulos, C., Yang, E., Estroff, J.A., Warfield, S.K., 2017. A normative spatiotemporal MRI atlas of the fetal brain for automatic segmentation and analysis of early brain growth. Scientific Reports 2017 7:1 7, 1–13.

[24] Goriely, A., Ben Amar, M., 2005. Differential growth and instability in elastic shells. Physical Review Letters .

[25] Guerrini, R., Dobyns, W., Barkovich, A., 2008. Abnormal development of the human cerebral cortex: genetics, functional consequences and treatment options. Trends in neurosciences 31, 154–162.

[26] Heuer, K., Gulban, O.F., Bazin, P.L., Osoianu, A., Valabregue, R., Santin, M., Herbin, M., Toro, R., 2019. Evolution of neocortical folding: A phylogenetic comparative analysis of MRI from 34 primate species. Cortex 118, 275–291.

[27] Holland, M.A., Miller, K.E., Kuhl, E., 2015. Emerging Brain Morphologies from Axonal Elongation. Annals of Biomedical Engineering 2015 43:7 43, 1640–1653.

[28] Keraudren, K., Kuklisova-Murgasova, M., Kyriakopoulou, V., Malamateniou, C., Rutherford, M., Kainz, B., Hajnal, J., Rueckert, D., 2014. Automated fetal brain segmentation from 2d mri slices for motion correction. NeuroImage 101, 633–643.

[29] Knutsen, A., Kroenke, C., Chang, Y., Taber, L., Bayly, P., 2013. Spatial and temporal variations of cortical growth during gyrogenesis in the developing ferret brain. Cerebral cortex (New York, N.Y. : 1991) 23, 488–498.

[30] Kriegstein, A., Noctor, S., Martínez-Cerdeño, V., 2006. Patterns of neural stem and progenitor cell division may underlie evolutionary cortical expansion.

[31] Kroenke, C.D., Bayly, P.V., 2018. How forces fold the cerebral cortex. Journal of Neuroscience .

[32] Kuklisova-Murgasova, M., Quaghebeur, G., Rutherford, M.A., Hajnal, J.V., Schnabel, J.A., 2012. Reconstruction of fetal brain mri with intensity matching and complete outlier removal. Medical Image Analysis 16, 1550–1564.

[33] Kyriakopoulou, V., Vatansever, D., Elkommos, S., Dawson, S., McGuinness, A., Allsop, J., MolnÃąr, Z., Hajnal, J., Rutherford, M., 2013. Cortical Overgrowth in Fetuses With Isolated Ventriculomegaly. Cerebral Cortex 24, 2141–2150.

[34] Lefèvre, J., Mangin, J.F., 2010. A Reaction-Diffusion Model of Human Brain Development. PLOS Computational Biology 6, e1000749.

[35] LefÃĺvre, J., Germanaud, D., Fischer, C., Toro, R., RiviÃĺre, D., Coulon, O., 2012. Fast surface-based measurements using first eigenfunction of the laplace-beltrami operator: Interest for sulcal description, in: 2012 9th IEEE International Symposium on Biomedical Imaging (ISBI), pp. 1527–1530.

[36] Li, L., Sinclair, M., Makropoulos, A., Hajnal, J.V., David Edwards, A., Kainz, B., Rueckert, D., Alansary, A., 2021. CAS-Net: Conditional Atlas Generation and Brain Segmentation for Fetal MRI. Lecture Notes in Computer Science (including subseries Lecture Notes in Artificial Intelligence and Lecture Notes in Bioinformatics) 12959 LNCS, 221–230.

[37] Lluch, È., De Craene, M., Bijnens, B., Sermesant, M., Noailly, J., Camara, O., Morales, H., 2019. Breaking the state of the heart: meshless model for cardiac mechanics. Biomechanics and Modeling in Mechanobiology 18.

[38] Maillot, J., Yahiaz, H., Verroustz, A., 1993. Interactive texture mapping. Proceedings of the 20th Annual Conference on Computer Graphics and Interactive Techniques, SIGGRAPH 1993 , 27–34.

[39] Makropoulos, A., Gousias, I.S., Ledig, C., Aljabar, P., Serag, A., Hajnal, J.V., Edwards, A.D., Counsell, S.J., Rueckert, D., 2014. Automatic whole brain mri segmentation of the developing neonatal brain. ieee transactions on medical imaging. IEEE Transactions on Medical Imaging 33, 1567–74.

[40] Makropoulos, A., Robinson, E.C., Schuh, A., Wright, R., Fitzgibbon, S., Bozek, J., Counsell, S.J., Steinweg, J., Vecchiato, K., Passerat-Palmbach, J., Lenz, G., Mortari, F., Tenev, T., Duff, E.P., Bastiani, M., Cordero-Grande, L., Hughes, E., Tusor, N., Tournier, J.D., Hutter, J., Price, A.N., Teixeira, R.P.A., Murgasova, M., Victor, S., Kelly, C., Rutherford, M.A., Smith, S.M., Edwards, A.D., Hajnal, J.V., Jenkinson, M., Rueckert, D., 2018. The developing human connectome project: A minimal processing pipeline for neonatal cortical surface reconstruction. NeuroImage .

[41] Messinger, A., Sirmpilatze, N., Heuer, K., Loh, K.K., Mars, R.B., Sein, J., Xu, T., Glen, D., Jung, B., Seidlitz, J., Taylor, P., Toro, R., Garza-Villarreal, E.A., Sponheim, C., Wang, X., Benn, R.A., Cagna, B., Dadarwal, R., Evrard, H.C., Garcia-Saldivar, P., Giavasis, S., Hartig, R., Lepage, C., Liu, C., Majka, P., Merchant, H., Milham, M.P., Rosa, M.G., Tasserie, J., Uhrig, L., Margulies, D.S., Klink, P.C., 2021. A collaborative resource platform for non-human primate neuroimaging. NeuroImage 226, 117519.

[42] Mill, J., Agudelo, V., Hion Li, C., Noailly, J., Freixa, X., Camara, O., , Dabit Arzamendi, 2021. Patient-specific flow simulation analysis to predict device-related thrombosis in left atrial appendage occluders. REC: interventional cardiology (English Edition) .

[43] Mota, B., Herculano-Houzel, S., 2015. Cortical folding scales universally with surface area and thickness, not number of neurons. Science 349, 74–77.

[44] Nie, J., Guo, L., Li, G., Faraco, C., Stephen Miller, L., Liu, T., 2010. A computational model of cerebral cortex folding. Journal of Theoretical Biology 264, 467–478.

[45] Niederer, S.A., Lumens, J., Trayanova, N.A., 2018. Computational models in cardiology. Nature Reviews Cardiology 2018 16:2 16, 100–111.

[46] Payette, K., de Dumast, P., Kebiri, H., Ezhov, I., Paetzold, J.C., Shit, S., Iqbal, A., Khan, R., Kottke, R., Grehten, P., Ji, H., Lanczi, L., Nagy, M., Beresova, M., Nguyen, T.D., Natalucci, G., Karayannis, T., Menze, B., Bach Cuadra, M., Jakab, A., 2021. An automatic multi-tissue human fetal brain segmentation benchmark using the Fetal Tissue Annotation Dataset. Scientific Data 2021 8:1 8, 1–14.

[47] Petitjean, S., 2002. A survey of methods for recovering quadrics in triangle meshes. ACM Comput. Surv. 34, 211–262.

[48] Raybaud, C., Ahmad, T., Rastegar, N., Shroff, M., Al Nassar, M., 2013. The premature brain: Developmental and lesional anatomy.

[49] Reillo, I., De Juan Romero, C., García-Cabezas, M.Á., Borrell, V., 2011. A Role for intermediate radial glia in the tangential expansion of the mammalian cerebral cortex. Cerebral Cortex .

[50] Richman, D.P., Stewart, R.M., Hutchinson, J.W., Caviness, V.S., 1975. Mechanical model of brain convolutional development. Science 189, 18–21.

[51] Robinson, E.C., Garcia, K., Glasser, M.F., Chen, Z., Coalson, T.S., Makropoulos, A., Bozek, J., Wright, R., Schuh, A., Webster, M., Hutter, J., Price, A., Cordero Grande, L., Hughes, E., Tusor, N., Bayly, P.V., Van Essen, D.C., Smith, S.M., Edwards, A.D., Hajnal, J., Jenkinson, M., Glocker, B., Rueckert, D., 2018. Multimodal surface matching with higher-order smoothness constraints. NeuroImage 167, 453–465.

[52] Robinson, E.C., Jbabdi, S., Glasser, M.F., Andersson, J., Burgess, G.C., Harms, M.P., Smith, S.M., Van Essen, D.C., Jenkinson, M., 2014. MSM: A new flexible framework for multimodal surface matching. NeuroImage .

[53] Routier, A., Burgos, N., Díaz, M., Bacci, M., Bottani, S., El-Rifai, O., Fontanella, S., Gori, P., Guillon, J., Guyot, A., Hassanaly, R., Jacquemont, T., Lu, P., Marcoux, A., Moreau, T., Samper-González, J., Teichmann, M., Thibeau-Sutre, E., Vaillant, G., Wen, J., Wild, A., Habert, M.O., Durrleman, S., Colliot, O., 2021. Clinica: An Open-Source Software Platform for Reproducible Clinical Neuroscience Studies. Frontiers in Neuroinformatics 0, 39.

[54] Rusinkiewicz, S., 2004. Estimating curvatures and their derivatives on triangle meshes, in: Proceedings. 2nd International Symposium on 3D Data Processing, Visualization and Transmission. 2004. 3DPVT 2004., pp. 486–493.

[55] Salomon, L., Bernard, J., Ville, Y., 2007. Reference ranges for fetal ventricular width: a non-normal approach. Ultrasound in obstetrics and gynecology : the official journal of the International Society of Ultrasound in Obstetrics and Gynecology 30, 61–66.

[56] Scott, J.A., Habas, P.A., Rajagopalan, V., Kim, K., Barkovich, A.J., Glenn, O.A., Studholme, C., 2012. Volumetric and surface-based 3d mri analyses of fetal isolated mild ventriculomegaly. Brain Structure and Function 2012 218:3 218, 645–655.

[57] Sun, T., Hevner, R.F., 2014. Growth and folding of the mammalian cerebral cortex: from molecules to malformations.

[58] Tallinen, T., Chung, J.Y., Biggins, J.S., Mahadevan, L., 2014. Gyrification from constrained cortical expansion. Proceedings of the National Academy of Sciences of the United States of America .

[59] Tallinen, T., Chung, J.Y., Rousseau, F., Girard, N., Lefèvre, J., Mahadevan, L., 2016. On the growth and form of cortical convolutions. Nature Physics .

[60] Toro, R., Burnod, Y., 2005. A morphogenetic model for the development of cortical convolutions. Cerebral Cortex 15, 1900–1913.

[61] Van Essen, D.C., 1997. A tension-based theory of morphogenesis and compact wiring in the central nervous system.

[62] Van Essen, D.C., 2020. A 2020 view of tension-based cortical morphogenesis. Proceedings of the National Academy of Sciences 117, 32868–32879.

[63] Vasung, L., Lepage, C., RadoÅą, M., Pletikos, M., Goldman, J.S., Richiardi, J., RaguÅ¿, M., Fischi-GÃşmez, E., Karama, S., Huppi, P.S., Evans, A.C., Kostovic, I., 2016. Quantitative and qualitative analysis of transient fetal compartments during prenatal human brain development.

Frontiers in Neuroanatomy 10, 11.

[64] Wang, S., Demirci, N., Holland, M.A., 2020. Numerical investigation of biomechanically coupled growth in cortical folding. Biomechanics and Modeling in Mechanobiology 2020 20:2 20, 555–567.

[65] Wang, X., 2021. Modélisation et caractérisation du plissement cortical. Ph.D. thesis. Ecole nationale supÃĪrieure Mines-TÃĪlÃĪcom Atlantique Bretagne Pays de la Loire.

[66] Wang, X., Bohi, A., Harrach, M.A., Dinomais, M., Lefevre, J., Rousseau, F., 2019. On early brain folding patterns using biomechanical growth modeling. 2019 41st Annual International Conference of the IEEE Engineering in Medicine and Biology Society (EMBC) , 146–149.

[67] Wang, X., Lefèvre, J., Bohi, A., Harrach, M.A., Dinomais, M., Rousseau, F., 2021. The influence of biophysical parameters in a biomechanical model of cortical folding patterns. Scientific Reports 11, 1–15.

[68] Welker, W., 1990. Why does cerebral cortex fissure and fold ? a review of determinants of gyri and sulci, in: Cerebral Cortex, pp. 3–136.

[69] Wyburd, M.K., Jenkinson, M., Namburete, A.I.L., 2020. Cortical Plate Segmentation Using CNNs in 3D Fetal Ultrasound. Communications in Computer and Information Science 1248 CCIS, 56–68.

[70] Xu, G., Knutsen, A.K., Dikranian, K., Kroenke, C.D., Bayly, P.V., Taber, L.A., 2010. Axons pull on the brain, but tension does not drive cortical folding. Journal of Biomechanical Engineering .

[71] Yezzi, A., Prince, J., 2003. An eulerian pde approach for computing tissue thickness. IEEE Transactions on Medical Imaging 22, 1332–1339.

[72] Zarzor, M., Kaessmair, S., Steinmann, P., Blümcke, I., Budday, S., 2021. A two-field computational model couples cellular brain development with cortical folding. Brain Multiphysics 2, 100025.

Declaration of interests

☒The authors declare that they have no known competing financial interests or personal relationships that could have appeared to influence the work reported in this paper.

☐The authors declare the following financial interests/personal relationships which may be considered as potential competing interests: